COQ6 mutations in human patients produce nephrotic syndrome with sensorineural deafness

Saskia F. Heeringa,[1] Gil Chernin,[1] Moumita Chaki,[1] Weibin Zhou,[1] Alexis J. Sloan,[2] Ziming Ji,[3] Letian X. Xie,[3] Leonardo Salviati,[4] Toby W. Hurd,[1] Virginia Vega-Warner,[1] Paul D. Killen,[5] Yehoash Raphael,[5] Shazia Ashraf,[1] Bugsu Ovunc,[1] Dominik S. Schoeb,[1] Heather M. McLaughlin,[1,6] Rannar Airik,[1] Christopher N. Vlangos,[1] Rasheed Gbadegesin,[1] Bernward Hinkes,[1,7] Pawaree Saisawat,[1] Eva Trevisson,[4] Mara Doimo,[4] Alberto Casarin,[4] Vanessa Pertegato,[4] Gianpietro Giorgi,[4] Holger Prokisch,[8,9] Agnès Rötig,[10] Gudrun Nürnberg,[11,12,13] Christian Becker,[11] Su Wang,[5] Fatih Ozaltin,[14] Rezan Topaloglu,[14] Aysin Bakkaloglu,[14] Sevcan A. Bakkaloglu,[15] Dominik Müller,[16] Antje Beissert,[17] Sevgi Mir,[18] Afig Berdeli,[18] Seza Özen,[14] Martin Zenker,[19] Verena Matejas,[7] Carlos Santos-Ocaña,[20] Placido Navas,[20] Takehiro Kusakabe,[21] Andreas Kispert,[22] Sema Akman,[23] Neveen A. Soliman,[24] Stefanie Krick,[2] Peter Mundel,[2] Jochen Reiser,[2] Peter Nürnberg,[11,12,13] Catherine F. Clarke,[3] Roger C. Wiggins,[5] Christian Faul,[2] and Friedhelm Hildebrandt[1,6,25]

[1]Department of Pediatrics, University of Michigan, Ann Arbor, Michigan, USA. [2]Department of Medicine, University of Miami Miller School of Medicine, Miami, Florida, USA. [3]Department of Chemistry and Biochemistry and Molecular Biology Institute, UCLA, Los Angeles, California, USA. [4]Department of Pediatrics, University of Padua, Padua, Italy. [5]Department of Internal Medicine, Department of Pathology, and Department of Otolaryngology and [6]Department of Human Genetics, University of Michigan, Ann Arbor, Michigan, USA. [7]Institute of Human Genetics, University Hospital of Erlangen, Erlangen, Germany. [8]Institute of Human Genetics, Helmholtz Zentrum Munich, German Research Center for Environmental Health, Neuherberg, Germany. [9]Institute of Human Genetics, Klinikum rechts der Isar, Technical University Munich, Munich, Germany. [10]INSERM U781, Hôpital Necker-Enfants Malade, Université René Descartes, Paris, France. [11]Cologne Center for Genomics, [12]Center for Molecular Medicine Cologne (CMMC), and [13]Cologne Excellence Cluster on Cellular Stress Responses in Aging-Associated Diseases (CECAD), University of Cologne, Cologne, Germany. [14]Department of Pediatric Nephrology, Hacettepe University, Ankara, Turkey. [15]Department of Pediatric Nephrology, Gazi University Faculty of Medicine, Ankara, Turkey. [16]Department of Pediatric Nephrology, Charité, Berlin, Germany. [17]University Children's Hospital, Würzburg, Germany. [18]Department of Pediatrics, Ege University, Izmir, Turkey. [19]Institute of Human Genetics, University Hospital of Magdeburg, Magdeburg, Germany. [20]Centro Andaluz de Biología del Desarrollo, Universidad Pablo de Olavide-CSIC and CIBERER, ISCIII, Seville, Spain. [21]Department of Biology, Faculty of Science and Engineering, Konan University, Kobe, Japan. [22]Institut für Molekularbiologie, Medizinische Hochschule Hannover, Hannover, Germany. [23]Department of Pediatric Nephrology, Akdeniz University, School of Medicine, Antalya, Turkey. [24]Department of Pediatrics, Kasr Alainy School of Medicine, Cairo University, Cairo, Egypt. [25]Howard Hughes Medical Institute, University of Michigan, Ann Arbor, Michigan, USA.

Steroid-resistant nephrotic syndrome (SRNS) is a frequent cause of end-stage renal failure. Identification of single-gene causes of SRNS has generated some insights into its pathogenesis; however, additional genes and disease mechanisms remain obscure, and SRNS continues to be treatment refractory. Here we have identified 6 different mutations in coenzyme Q_{10} biosynthesis monooxygenase 6 (*COQ6*) in 13 individuals from 7 families by homozygosity mapping. Each mutation was linked to early-onset SRNS with sensorineural deafness. The deleterious effects of these human *COQ6* mutations were validated by their lack of complementation in *coq6*-deficient yeast. Furthermore, knockdown of *Coq6* in podocyte cell lines and *coq6* in zebrafish embryos caused apoptosis that was partially reversed by coenzyme Q_{10} treatment. In rats, COQ6 was located within cell processes and the Golgi apparatus of renal glomerular podocytes and in stria vascularis cells of the inner ear, consistent with an oto-renal disease phenotype. These data suggest that coenzyme Q_{10}–related forms of SRNS and hearing loss can be molecularly identified and potentially treated.

Introduction

Nephrotic syndrome (NS), a malfunction of the kidney glomerular filter, leads to proteinuria, hypoalbuminemia, and edema. Steroid-resistant NS (SRNS) represents a frequent cause of end-stage renal failure (ESRF), which requires renal replacement therapy for survival. Identification of single-gene causes of NS (1–7) has generated the first insights (8, 9) into its pathogenesis: (a) that single-gene causes of NS result in SRNS (10, 11) with very few exceptional cases that respond to treatment (3, 12); (b) that SRNS-causing genes are expressed in a specialized cell type, the glomerular podocyte (13); and (c) that the pathohistology ranges from the intrauterine-onset severe developmental phenotype of diffuse mesangial sclerosis (DMS) to the childhood-onset phenotype of focal segmental glomerulosclerosis (FSGS). Two-thirds of all SRNS cases with onset in the first year of life (14) and 10%–28% of all childhood cases (15) are caused by single-gene mutations in 1 of only 4 genes, *NPHS1* (1), *NPHS2* (2), *LAMB2* (16), and *WT1* (17). However, the molecular cause of more than 80% of all cases of SRNS is unknown, and treatment options have yet to be discovered. We therefore performed total genome search for linkage to identify further causative recessive genes.

Authorship note: Saskia F. Heeringa and Gil Chernin contributed equally to this work.

Conflict of interest: The authors have declared that no conflict of interest exists.

Citation for this article: *J Clin Invest.* 2011;121(5):2013–2024. doi:10.1172/JCI45693.

Results

COQ6 mutations cause SRNS with sensorineural deafness (SND). To identify further single-gene causes for SRNS, we performed a genome-wide search for linkage in 14 different consanguineous families with SRNS. Calculating lod under the hypothesis of locus heterogeneity yielded a significant maximum heterogeneity lod score of 4.9 (α = 52%) on human chromosome 14q24.3, covering a region of 6.4 Mb (Figure 1A). Of 7 families homozygous at this locus (*SRNS2*), families A1072 and F1082 from Turkey revealed haplotype sharing (Figure 1B), restricting the critical genetic region to 2.1 Mb under the hypothesis that an ancestor common to both families introduced the disease allele (i.e., homozygosity by descent). This interval contained 32 positional candidate genes (Figure 1C).

Exon sequencing of *COQ6* yielded homozygous mutations in 3 of the 7 families homozygous at the *SRNS2* locus (Table 1). In both affected individuals of family A1072, we detected a homozygous A353D substitution (Figure 1G and Table 1) that was also found in family F1082, as predicted from haplotype sharing at *SRNS2* (Figure 1B). All 3 affected individuals that were examined in the northern Lebanese family F252 exhibited the homozygous change G255R (Figure 1G and Table 1). This mutation was shared by 3 affected individuals of family A234 from southern Turkey (Table 1), most likely as a founder effect. Both missense mutations altered amino acid residues that are uniformly conserved from *E. coli* to humans (Figure 1G). Another individual with SRNS from Turkey revealed 2 compound heterozygous truncating mutations, W447X and Q461fsX478 (Figure 1G and Table 1). All mutations were absent from more than 90 healthy control subjects from central Europe and 60 healthy control subjects from Turkey. Segregation of mutations was consistent with recessive inheritance (Table 1). In all 9 individuals with SRNS that were examined for hearing loss, there was SND (Table 1). Exon sequencing of all other 31 genes at the *SRNS2* locus did not yield any mutations in the families F252, F1082, and A1072. We thus identified mutations in *COQ6* as a cause of recessive early-onset SRNS with SND (NPHS type 5), which we believe to be novel.

We then performed exon PCR of *COQ6* in another 530 families: 70 with SRNS, 35 that were homozygous for 3 markers at the *COQ6* locus, 55 with a neurologic phenotype, and 370 with a mitochondriopathy. We identified a single heterozygous nonsense mutation, R162X, in A988-21, an individual with cyclosporine A–dependent (CsA-dependent) NS, and a single heterozygous nonsense mutation, W188X, in A1904-21, an individual with DMS (Figure 1G). As NPHS type 5 appears recessive, the second mutation most likely escaped identification in these 2 families.

All 11 affected individuals of the 5 families with 2 recessive *COQ6* mutations had SRNS. They manifested with proteinuria at a median age of 1.2 years (range, 0.2–6.4 years) and progressed to ESRF by a median age of 1.7 years (range, 0.4–9.3 years); 5 individuals died in early childhood (median age, 5.0 years). Renal biopsy revealed FSGS in 7 cases (Table 1 and Figure 2, A–C) and DMS in 1 case. Subject A234-21 presented with seizures, and subject F1082-21 had white matter abnormalities and seizures and died of multiorgan failure in sepsis; 2 other individuals had ataxia and facial dysmorphism (individuals F252-51 and A234-26, respectively; Table 1).

COQ6 function. The *COQ6* gene extends over 13.2 kb and contains 12 exons (Figure 1, D and E). There are 18 putative isoforms resulting from alternative splicing (www.aceview.org). Full-length isoforms a and b contain 12 exons, but use alternative exons 1a and 1b (Supplemental Figure 1, A and B; supplemental material available online with this article; doi:10.1172/JCI45693DS1). Full-length isoforms were expressed in multiple tissues, including the kidney (Supplemental Figure 1, C–F). Using in situ hybridization analysis, we demonstrated *Coq6* mRNA expression in the metanephric mesenchyme and forming nephrons of mouse kidney (Supplemental Figure 1, G–L). Isoform a (encoding a 54-kDa protein) is predicted to be expressed in mitochondria with a Predotar score of 0.81 (http://urgi.versailles.inra.fr/predotar) because of a mitochondrial leader peptide, whereas isoform b (encoding a 51-kDa protein), which uses an alternative exon 1, is considered only possibly mitochondrial, with a Predotar score of 0.45. Both isoforms encode a flavin-dependent monooxygenase with 3 flavin adenine dinucleotide–binding motifs (18). The amino acid sequence is highly conserved throughout evolution, with identity to the human COQ6 protein sequence of 66% for *Danio rerio* and 33% for the *E. coli* ortholog *UbiH*. The enzyme coenzyme Q_{10} monooxygenase 6 (COQ6) is required for biosynthesis of coenzyme Q_{10} (CoQ_{10}; also referred to as ubiquinone) and is thought to catalyze one or more ring hydroxylation steps. Humans synthesize CoQ_{10}, and yeast synthesizes CoQ_6 (where CoQ_n designates a polyisoprene residue with *n* isoprene units). CoQ_{10} operates as a redox carrier in the mitochondrial respiratory chain shuttling electrons from respiratory chain complexes RCCI and RCCII to complex RCCIII (19). CoQ_{10} also serves as a lipid-soluble antioxidant and has previously been implicated in protection from cell damage by ROS (20).

Because rare recessive mutations have been described in syndromic and nonsyndromic forms of NS (21, 22) in other genes involved in CoQ_{10} biosynthesis (23–25), we performed sequencing of all exons of the following 11 candidate genes: *PDSS1*, *PDSS2*, *COQ2*, *COQ3*, *COQ4*, *COQ5*, *COQ7*, *COQ8*, *COQ9*, *COQ10a*, and *COQ10b*. We examined 42 individuals with SRNS who had extrarenal symptoms suggestive of mitochondrial disease or in whom only 1 heterozygous *COQ6* mutation was found. However, we did not detect any further mutations. The 4 protein-truncating mutations in *COQ6* that we detected in subjects A988, A1904, and A3331-21 (Figure 1G and Table 1) may be considered null alleles. Similarly, the fully conserved homozygous missense mutations G225R and A353D that we observed in 4 families with SRNS and SND may also represent loss-of-function mutations (Figure 1G and Table 1). To test this hypothesis, we examined all 6 *COQ6* mutations for potential deleterious effects by complementation in *coq6*-deficient yeast strains. Yeast cells harboring a deletion mutation in the *coq6* gene were unable to grow on yeast extract/peptone/glycerol media (YPG; in which glycerol acts as a nonfermentable carbon source) and were deficient in CoQ_6 (Figure 2, D and E, and ref. 18). Expression of human WT *COQ6* with an aminoterminal yeast mitochondrial leader sequence rescued both YPG growth and CoQ_6 content (Figure 2, D and E), although not as robustly as did yeast harboring the WT *COQ6* gene (pSR1-1; Figure 2, D and E). Rescue of growth on YPG was observed with either low–copy number (pQM; Figure 2D) or high–copy number (pRCM; data not shown) expression constructs. Both constructs also rescued the deficiency in CoQ_6 content (Figure 2E). In contrast, none of the *Coq6* constructs harboring the human mutations (Figure 1G and Table 1) were able to rescue the growth deficiency phenotype or CoQ_6 content phenotypes (Figure 2, D and E), thereby demonstrating the deleterious effects of these mutations.

Response to CoQ_{10} treatment. Monogenic variants of childhood NS are characterized by a lack of response to therapy (26). Because successful CoQ_{10} treatment had been described previously in an

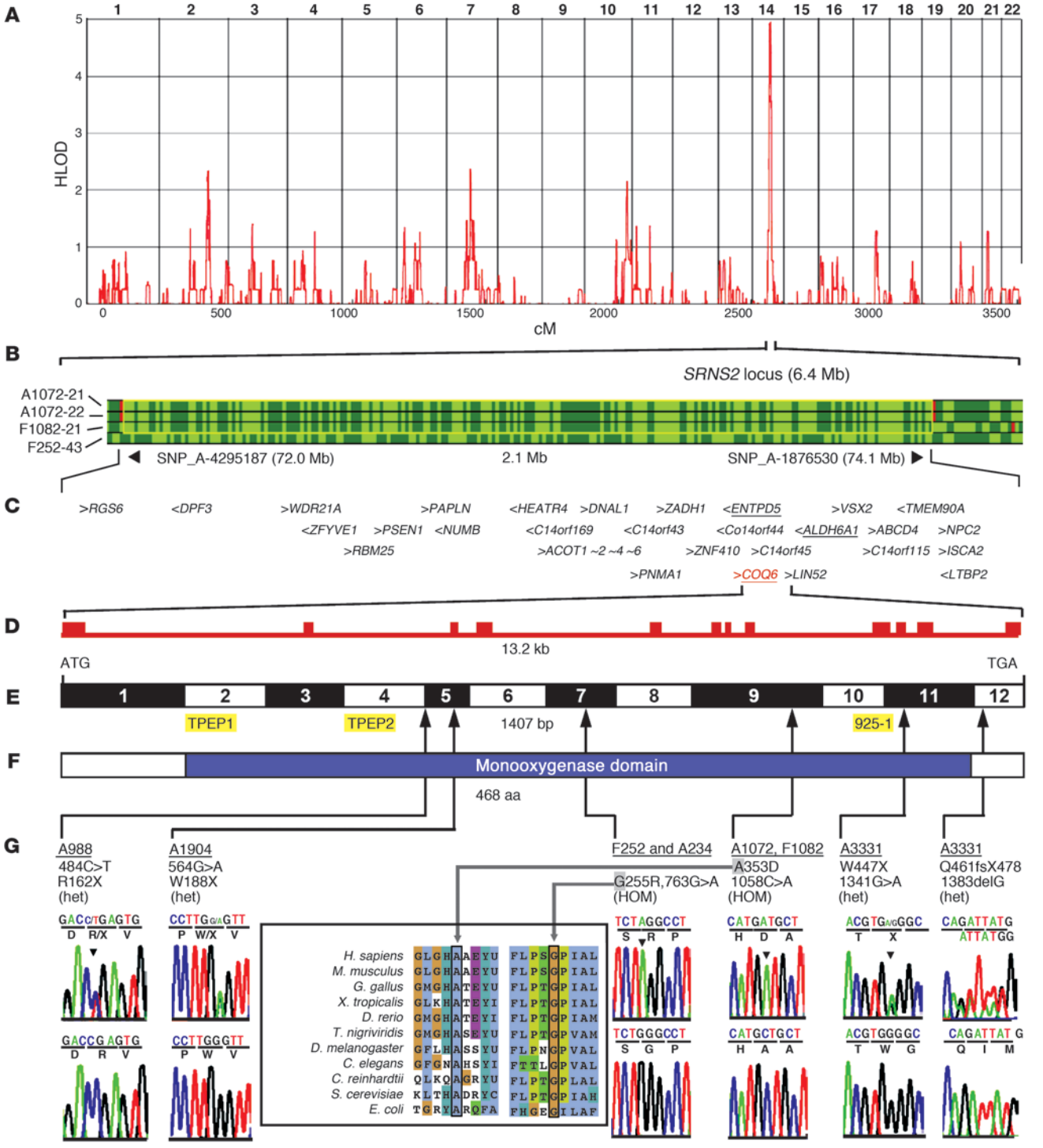

Figure 1

Positional cloning of *COQ6* mutations in individuals with NS and SND. (**A**) lod score profile across the human genome in affected children from 14 consanguineous kindred with SRNS. Parametric heterogeneity lod (HLOD) scores are plotted against human chromosomal mapping positions, concatenated from p-ter (left) to q-ter (right). (**B**) Within the *SRNS2* locus, haplotypes from 250k SNP analysis are shown for 3 of the 7 families with homozygosity at the *SRNS2* locus. Alleles are colored light green (AA), dark green (BB), and red (AB). (**C**) The 32 genes within the *SRNS2* locus; 3 genes preferentially expressed in kidney podocytes are underlined. Mutations were found in *COQ6*. Transcriptional direction is indicated by < or >. (**D**) *COQ6* extends over 13.2 kb and contains 12 exons (boxes). (**E**) Exon structure of COQ6 cDNA. Arrows indicate relative positions of mutations (see **G**). Positions of peptides for antibody generation are shown in yellow. (**F**) Domain structure of COQ6 protein. Extent of the monooxygenase domain is shown in relation to encoding exon position (**E**). (**G**) 6 different *COQ6* mutations in 7 families with SRNS. Family number and amino acid change (see Table 1) are given above sequence traces. Arrows denote positions of mutations in relation to exons and protein domains. For the 2 missense mutations, G255R and A363D, full conservation across evolution of altered amino acid residues is illustrated.

Table 1
Recessive *COQ6* mutations detected in 5 families with NS and deafness

Patient ID	Origin	Consang	Nucleotide mutation	Protein sequence change[A]	Exon (segregation)[B]	Age at onset (yr)	Age at ESRF (yr)	Kidney disease/ treatment[C]	Histology (at yr of age)	Extrarenal manifestations
F252-43	Lebanon	Y	763G>A	G255R	7 (hom,M,P)	6.4	9.3	SRNS	FSGS (6.8)	Congenital SND
F252-46	Lebanon	Y	763G>A	G255R	7 (hom,M,P)	0.3	1.7	SRNS	ND	Congenital SND (died 17.5 yr)
F252-51	Lebanon	Y	763G>A	G255R	7 (hom,M,P)	1.2	1.4	SRNS	FSGS (1.2)	SND, ataxia (died 6.5 yr)
F252-42	Lebanon	Y	ND	ND	7 (hom,M,P)	<1.0	3.0	SRNS, CP-R	FSGS (1.1)	Congenital SND (died 5.0 yr)
A234-21	Turkey	Y	763G>A	G255R	7 (hom,M,P)	0.3	0.4	SRNS	DMS	Seizures (died)
A234-26	Turkey	Y	763G>A	G255R	7 (hom,M,P)	0.3	0.4	SRNS, CoQ_{10}[D]	ND	SND, facial dysmorphism
A234-27	Turkey	Y	763G>A	G255R	7 (hom,M,P)	0.2	(none at 15 mo)	CoQ_{10}, ACE-I[D]	ND	SND (10 mo), bilateral nephrolithiasis (5 mo), GR
A1072-21	Turkey	Y	1058C>A	A353D	9 (hom,M,P)	6.0	6.5	SRNS, CP-R	FSGS (6)	SND (6 yr)
A1072-22	Turkey	Y	1058C>A	A353D	9 (hom,M,P)	2.5	NA	SRNS, CsA-S, CoQ_{10}[D]	FSGS (2.5)	SND (4 yr)
F1082-21	Turkey	Y	1058C>A	A353D	9 (hom,M,ND)	2.5	3.4	SRNS	FSGS (3)	Seizures, white matter abnormalities (died, sepsis)
A3331-21	Turkey	N	1341G>A	W447X	11 (het,P)	3.0	NA	SRNS, CP-R, ACE-I, levamizole	FSGS (3)	SND (40% of normal)
A3331-21	Turkey	N	1383delG[E]	Q461fsX478[E]	12 (het,M)	3.0	NA	SRNS, CP-R, ACE-I, levamizole	FSGS (3)	SND (40% of normal)

2 additional mutations (heterozygous only) were detected in families A998 (R162X) and A1904 (W188X) (see Figure 1G). ND, no data or DNA available. Consang, Consanguinity. [A]All mutations were absent from more than 90 healthy control subjects from Central Europe and from 60 healthy control subjects from Turkey. All missense mutations were conserved down to *E. coli*. [B]hom, homozygous in affected individual; het, heterozygous in affected individual; M, heterozygous mutation identified in mother; P, heterozygous mutation identified in father. [C]ACE-I, ACE inhibitor; CsA-S, CsA sensitive; CP-R, cyclophosphamide resistant; GR, growth retardation; CoQ_{10}, treatment with CoQ_{10}. [D]Treatment-sensitive case (renal replacement therapy not listed). [E]Isoform a.

individual with *COQ2* mutations (12), we administered CoQ_{10} in 2 children whose parents consented. Treatment was administered orally, giving 1 Softgel CoQ_{10} capsule (50 mg; GNC Preventive Nutrition) twice per day. Individual A234-27 presented with proteinuria without edema at 2 months of age, when the *COQ6* mutation was detected in his sister (A234-26) and cousin (A234-21). Urine protein/creatinine ratio was 40 mg/mg initially (normal, <0.2 mg/mg). Treatment was commenced at 2 months of age, giving CoQ_{10} orally at 15 mg/kg/d divided in 3 doses over 2 months together with enalapril (1.25 mg/d orally). CoQ_{10} treatment was then increased to 30 mg/kg/d, and urine protein/creatinine ratio decreased to 8 mg/mg within 2 months. Proteinuria decreased further to 5.8 mg/mg and remained stable at 4.8 mg/mg during the last follow-up at 15 months of age. Renal function was normal throughout. Bilateral severe SND and severe growth retardation were noted at 10 months. After treatment with 50 mg CoQ_{10} orally twice per day, SND substantially improved in A234-26. Individual A1072-22 manifested with NS at age 2.5 years. CoQ_{10} treatment was started at 5.5 years of age, when the subject was in partial remission from CsA treatment, which was discontinued at 5.8 years. At the beginning of CoQ_{10} treatment, 24-hour protein excretion was 7 mg/m^2/h (117 mg/d); 2 months into treatment, it decreased to 3.7 mg/m^2/h (76 mg/d), and remission was maintained at the end of the study period. Hearing was not improved after CoQ_{10} treatment. When CoQ_{10} treatment was inadvertently interrupted, proteinuria reappeared at a level of 57 mg/m^2/h (1,100 mg/d). Following reinstitution of CoQ_{10} treatment, proteinuria decreased again to 9 mg/m^2/h (188 mg/d).

Exogenous Coq6 localizes to mitochondria. To study the subcellular localization of COQ6, we generated GFP-labeled clones of human full-length isoforms a, b, and c (Supplemental Figure 1, A and B). We also generated anti-COQ6 antibodies directed against the synthetic peptides, whose positions in relation to exons and protein domains are shown in Figure 1E. Following affinity purification, antibody α–COQ6-TPEP2 detected a major band at the expected size of 50.8 kDa for full-length human COQ6 (Supplemental Figure 2). Because human full-length *COQ6* isoform a contains a putative mitochondrial leader sequence, we predicted that exogenous expression would result in mitochondrial localization. Indeed, after transient exogenous transfection into Cos-7 or HeLa cells or into murine podocyte cell lines, exogenous *COQ6* isoform a colocalized quantitatively in mitochondria with mitochondrial markers cytochrome *c* and cytochrome *c* oxidase (COXIV; Figure 3, A and B). Surprisingly, whereas α–COQ6-TPEP2 clearly detected exogenously expressed COQ isoform a, thereby confirming specificity of the antibody, it detected an additional endogenous signal that appeared to be localized in Golgi apparatus (Figure 3C). In fact, this endogenous signal detected by α–COQ6-TPEP2 was located in Golgi, as confirmed by double labeling with the Golgi marker Golgin 97 (Figure 3D). Interestingly, α–COQ6-TPEP2 did not reveal any endogenous COQ6 expression in mitochondria (Figure 3, D and E). Furthermore, exogenously

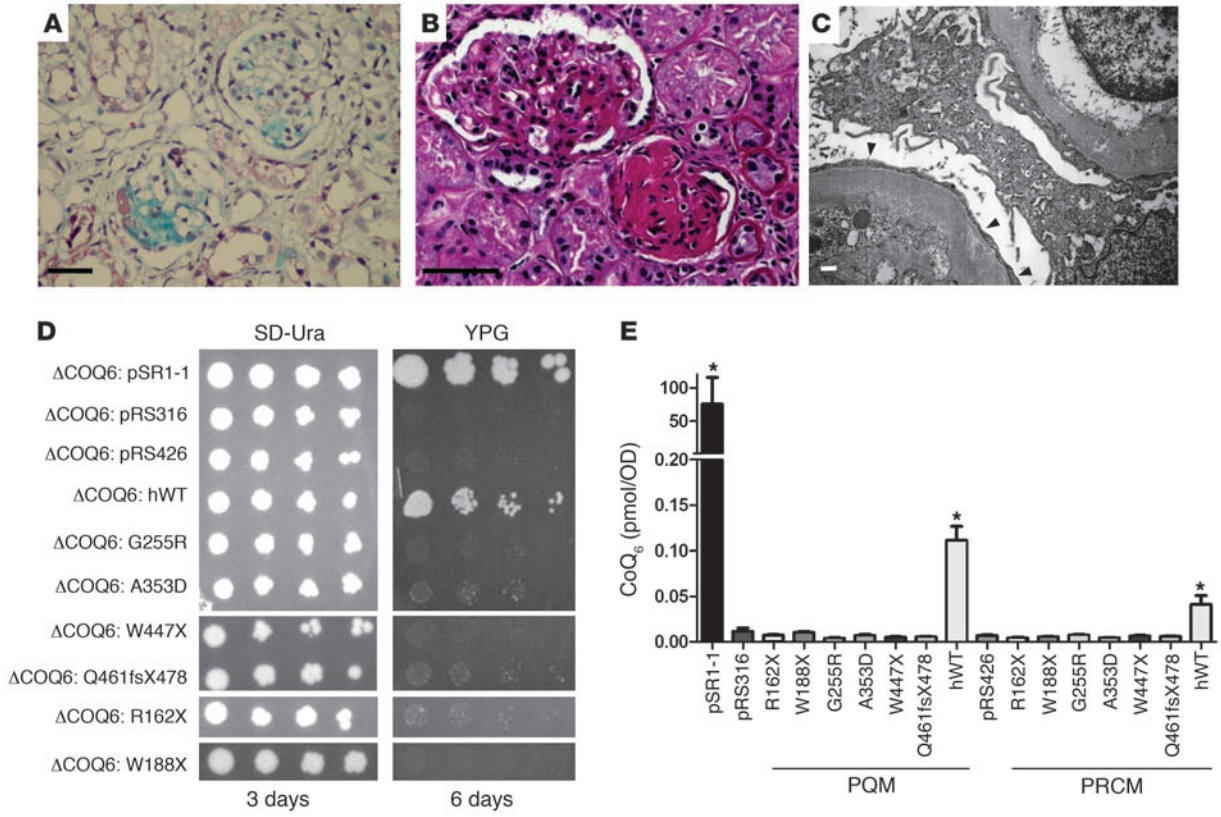

Figure 2

COQ6 loss-of-function causes glomerular damage in human kidney and growth defects in yeast. (**A**–**C**) Renal histology in individuals revealed homozygous *COQ6* mutation in A3331-21 FSGS, demonstrated by increased fibrosis (blue) in Trichrome-Masson staining (**A**), and in F1082-21, demonstrated by excess PAS staining (red) (**B**). (**C**) Transmission electron microscopy for F1082 showed effacement of podocyte foot processes, resulting in a continuous electron-dense layer (arrowheads). Scale bars: 50 μm (**A** and **B**); 250 nm (**C**). (**D** and **E**) Functional test of human *COQ6* mutations in yeast *coq6*-null mutants. (**D**) WT human *COQ6* (hWT), but not mutations, rescued growth in yeast *coq6*-null mutants plated on a nonfermentable carbon source. Yeast cells harboring the indicated low-copy plasmids were cultured in SD-Ura, seeded to both SD-Ura and YPG plate media, and incubated at 30°C for the times indicated. pSR1-1 contains the yeast *COQ6* gene (18) and served as positive control. Empty vectors pRS316 and pRS426 served as negative controls. (**E**) WT human *COQ6*, but not mutations, rescued CoQ_6 synthesis in yeast *coq6*-null mutants. CoQ_6 content of each yeast *coq6*-null mutant harboring 1 of the designated plasmids was determined as described in Methods. Each CoQ_6 measurement represents mean ± SD of 4 measurements from 2 independent samples. $^*P < 0.0005$ versus negative control (99% confidence level). PQM and PRCM indicate low– and high–copy number plasmids, respectively.

expressed full-length *COQ6* isoform a spared Golgi expression, as demonstrated with Giantin as a Golgi marker (Figure 3F). Likewise, in podocyte cell lines, the cell type central to the disease mechanism of SRNS, α–COQ6-TPEP2 detected endogenous COQ6 in Golgi, but not in mitochondria (Figure 3G). The endogenous COQ6 expression pattern was confirmed with the antibody α–COQ6–925-1 (Supplemental Figure 3, A and B), which was derived from a different peptide (Figure 1E).

Endogenous COQ6, COQ7, and COQ9 colocalize to cell processes and Golgi in rat podocytes. Monogenic forms of SRNS are caused by dysfunction of the glomerular podocyte, a terminally differentiated cell critical for the filtering function of the kidney glomerulus. (13, 26). We therefore examined expression of the COQ6 protein in kidney. COQ6 was seen almost exclusively in glomeruli, rather than in tubules (Figure 4A). As predicted, within glomeruli, COQ6 was expressed specifically in podocytes, as marked by WT1 labeling (Figure 4A). Within podocytes, COQ6 was absent from mitochondria (labeled with COXIV; Figure 4A); conversely, it was expressed within cellular processes and within Golgi apparatus (Figure 4, B and C), which confirmed the results obtained in cell lines (Figure 3). Because nonmitochondrial localization and function has been previously described for CoQ_6 (27), we hypothesized that nonmitochondrial expression would also apply to COQ7 and COQ9, which are known as mitochondrial proteins but share a multienzyme complex together with COQ6 for the biosynthesis of CoQ_{10} and CoQ_6 (21). Indeed, upon immunofluorescence, both COQ6 and COQ7 fully colocalized to cellular processes and Golgi of rat glomerular podocytes (Figure 4, B and C), as did COQ7 and COQ9 (Supplemental Figure 3C). We demonstrated specificity of this signal for α–COQ6-TPEP2 by showing the absence of the podocyte signal after preabsorption with the cognate peptide TPEP2, in contrast to its presence after preabsorption with the noncognate peptide TPEP1 (Supplemental Figure 3D). In addition, COQ6 colocalized to podocyte cellular processes with podocin (Figure 4E), another gene product that, if mutated, causes a Mendelian form of SRNS (2). These findings demonstrate that COQ6, COQ7, and COQ9 are all 3 expressed in cellular processes and Golgi apparatus of podocytes rather than in mitochondria.

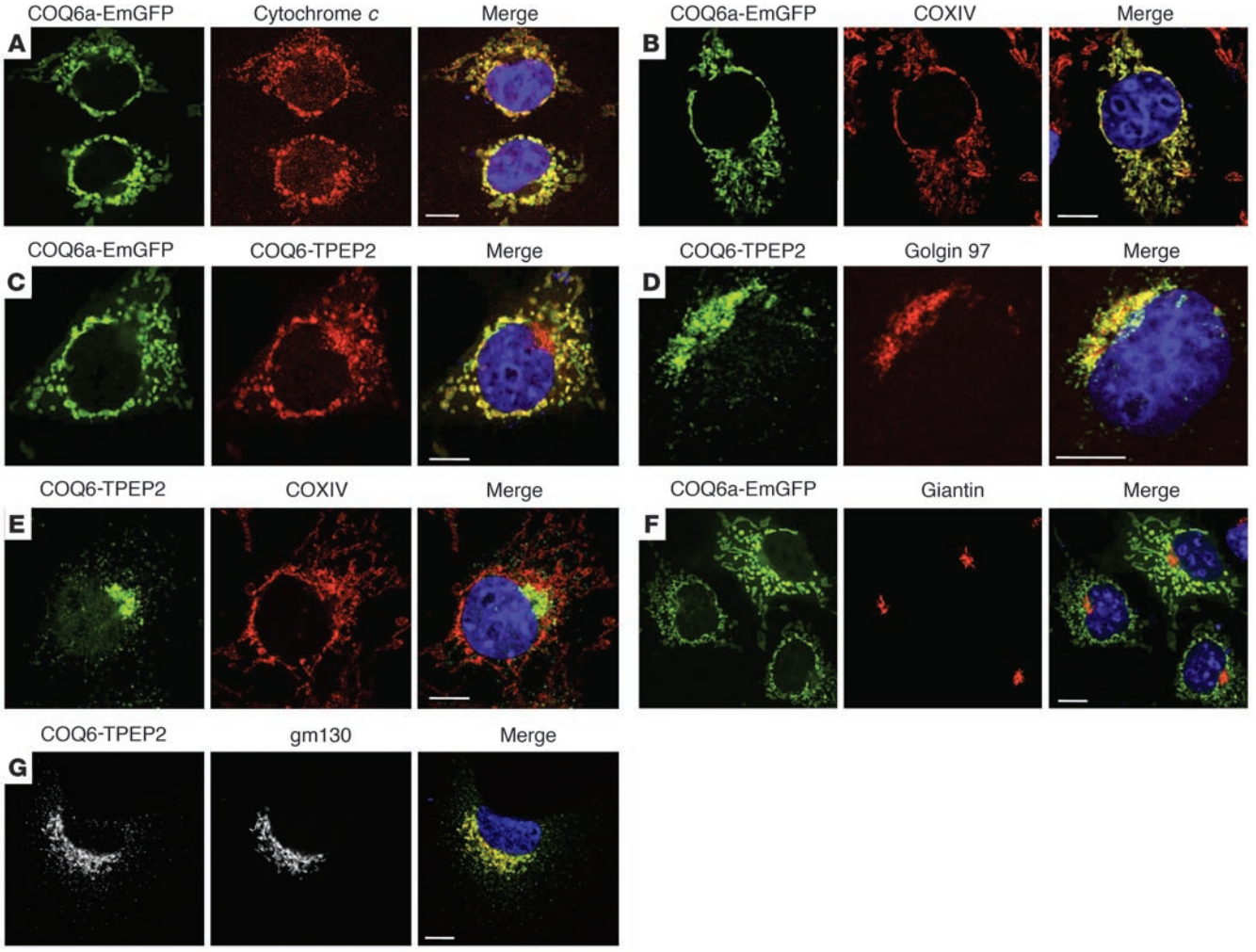

Figure 3

Transient exogenous expression of full-length human *COQ6* isoform a into Cos-7 cells, HeLa cells, or murine podocyte cell lines. (**A** and **B**) GFP-labeled full-length human *COQ6* isoform a (COQ6a-EmGFP) exogenously expressed in Cos-7 cells colocalized quantitatively with mitochondrial markers cytochrome *c* (**A**) and COXIV (**B**). (**C**–**E**) GFP-labeled full-length human *COQ6* isoform a expressed exogenously in HeLa cells was detected by α–COQ6-TPEP2 upon immunofluorescence, thereby confirming specificity of the antibody (**C**). α–COQ6-TPEP2 detected an additional endogenous signal, which appeared to be localized in Golgi apparatus (**C**), as confirmed by double labeling with Golgi marker Golgin 97 (**D**). α–COQ6-TPEP2 did not reveal any endogenous COQ6 expression in mitochondria (**D** and **E**). (**F**) GFP-labeled full-length human *COQ6* isoform a expressed exogenously in HeLa cells spared Golgi expression, as demonstrated with Giantin as a Golgi marker. (**G**) α–COQ6-TPEP2 detected endogenous COQ6 in Golgi of a podocyte cell line, as marked by gm130, but not in mitochondria. Scale bars: 5 μm.

We then investigated expression of COQ6 in the inner ear, because hearing loss is the other phenotype in this oto-renal syndrome. Immunofluorescence studies using α–COQ6-TPEP2 revealed COQ6 expression in the spiral ganglion as well as in cells of stria vascularis and spiral ligament (Figure 4, F and G), which are involved in maintaining the high potassium concentration in the cochlear duct necessary for sound transduction of the hair cells of Corti organ.

Coq6 knockdown in cultured podocytes induces apoptosis that is reversed by CoQ_{10} treatment. In order to study *COQ6* function in glomerular podocytes, the cell type involved in the disease phenotype, we performed knockdown of *Coq6* expression in vitro using a vector-based siRNA approach (28). Murine podocytes (29) were stably transfected with *COQ6* siRNA constructs, and clones were analyzed by RT-PCR for *Coq6* expression levels. We compared clones transfected using a scrambled siRNA oligonucleotide with non-transfected WT podocytes. The 3 clones that showed the highest degree of *Coq6* downregulation (clones 1, 2, and 5) were selected for functional studies (Supplemental Figure 1M). First, we analyzed the growth behavior of *Coq6* knockdown clones when kept in an undifferentiated and proliferative state (Figure 5A). When we seeded a defined number of cells and counted them after 24, 48, and 72 hours of cultivation, we found that the growth rate of the 3 *Coq6* knockdown clones was strongly decreased, while the scrambled siRNA clone C proliferated at the same rate as WT cells (Figure 5A). This difference reached statistical significance after 24 hours for clones 2 and 5 ($P < 0.05$) and after 72 hours for clone 1 ($P < 0.005$; Figure 5A). As the scrambled siRNA clone C did not

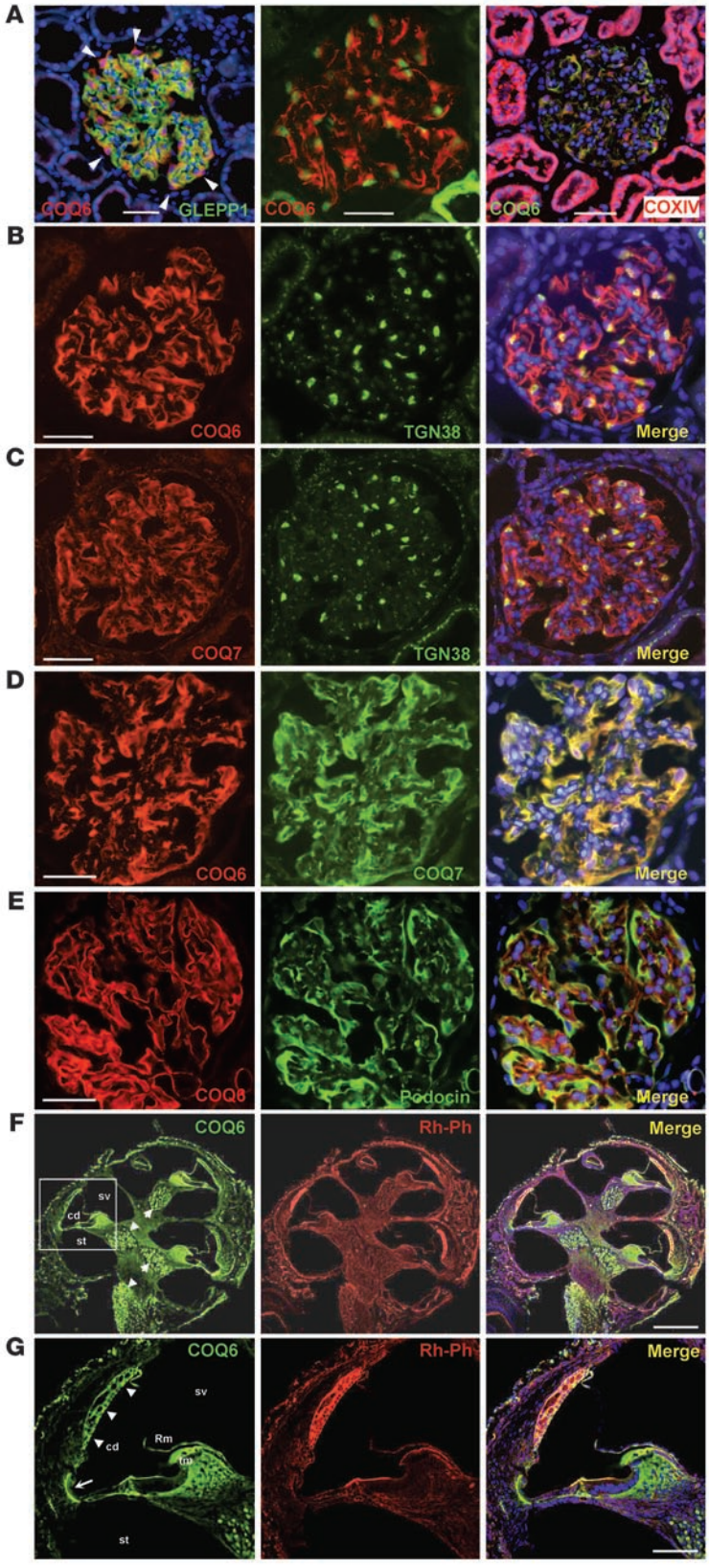

Figure 4
COQ6 and COQ7 colocalize in rat podocytes to cell processes and Golgi and in the inner ear to stria vascularis and spiral ligament cells. (**A**) In rat renal glomeruli (marked with an α-GLEPP1 antibody), α–COQ6-TPEP2 labeled podocyte cytoplasm and cell processes (left). COQ6 was expressed in podocytes, whose nuclei were marked with α-WT1 (middle), but not in mitochondria, marked with α-COXIV (right). (**B**) COQ6 (red) was located in podocyte cellular processes and in Golgi (marked with the trans-Golgi antibody TGN38), demonstrating colocalization (yellow). (**C**) COQ7 exhibited an expression pattern identical to that of COQ6 (see **B**). (**D**) There was full colocalization of COQ6 and COQ7 in podocyte cytoplasm, cell processes, and (by inference from **B** and **C**) Golgi. (**E**) COQ6 colocalized in podocyte cellular processes with podocin, another protein that, if mutated, causes SRNS. COQ6 showed additional expression more centrally in cell processes. (**F**) In cochlea (counterstained with rhodamin-phalloidin [Rh-Ph] for F-actin), COQ6 was expressed in spiral ganglion neurons in Rosenthal canal (arrowheads). (**G**) Higher-magnification view of boxed region in **F** showing COQ6 expression in stria vascularis cells (arrowheads) and the spiral ligament (arrow). Signal in tectorial membrane (tm) and adjacent structures most likely represents background staining. Rm, Reissner membrane; cd, cochlear duct; st, scala tympani; sv, scala vestibuli. In merged images, nuclei are stained blue with DAPI. Scale bars: 50 μm (**A**–**E**); 300 μm (**F**); 100 μm (**G**).

show any difference in growth behavior compared with WT podocytes, the scrambled clone was used as negative control for further experiments. To analyze whether the diminished overall growth rate in podocytes after *Coq6* knockdown is associated with activation of the intrinsic apoptotic pathway, we next determined the inner mitochondrial membrane potential ($\Delta\Psi m$) in these podocyte clones by using the fluorescent dye tetramethylrhodamine ethylester (TMRE). Compared with control cells, all 3 knockdown clones showed a substantial drop in TMRE fluorescence (data not shown), indicative of an increased percentage of podocytes with depolarized $\Delta\Psi m$.

We then analyzed activity of caspase-9 (Figure 5B), the major caspase downstream of mitochondria-mediated apoptosis (30). Using fluorometric immunosorbent enzyme assay (FIENA), we detected a more than 2-fold increase of caspase-9 activity in all 3 knockdown clones compared with control podocytes ($P < 0.005$; Figure 5B). Moreover, caspase-3, the final downstream executioner caspase of different apoptotic signaling pathways (31), showed significant elevation of activity for all 3 siRNA clones ($P < 0.05$; Figure 5C), consistent with the effect seen in zebrafish (see below). These data suggest that the observed decline in podocyte growth after *Coq6* knockdown is caused, at least in part, by increased apoptosis. Since mitochondria-induced apoptosis is associated with depolarization of the inner mitochondrial membrane (32) as well as caspase-9 activation (30), it is likely that lack of growth upon *Coq6* knockdown is caused by activation of the intrinsic apoptotic pathway. Because some of the SRNS patients in our study that carry *COQ6* mutations responded partially to CoQ_{10} treatment, we then analyzed whether CoQ_{10} has a beneficial effect on the phenotype caused by knockdown

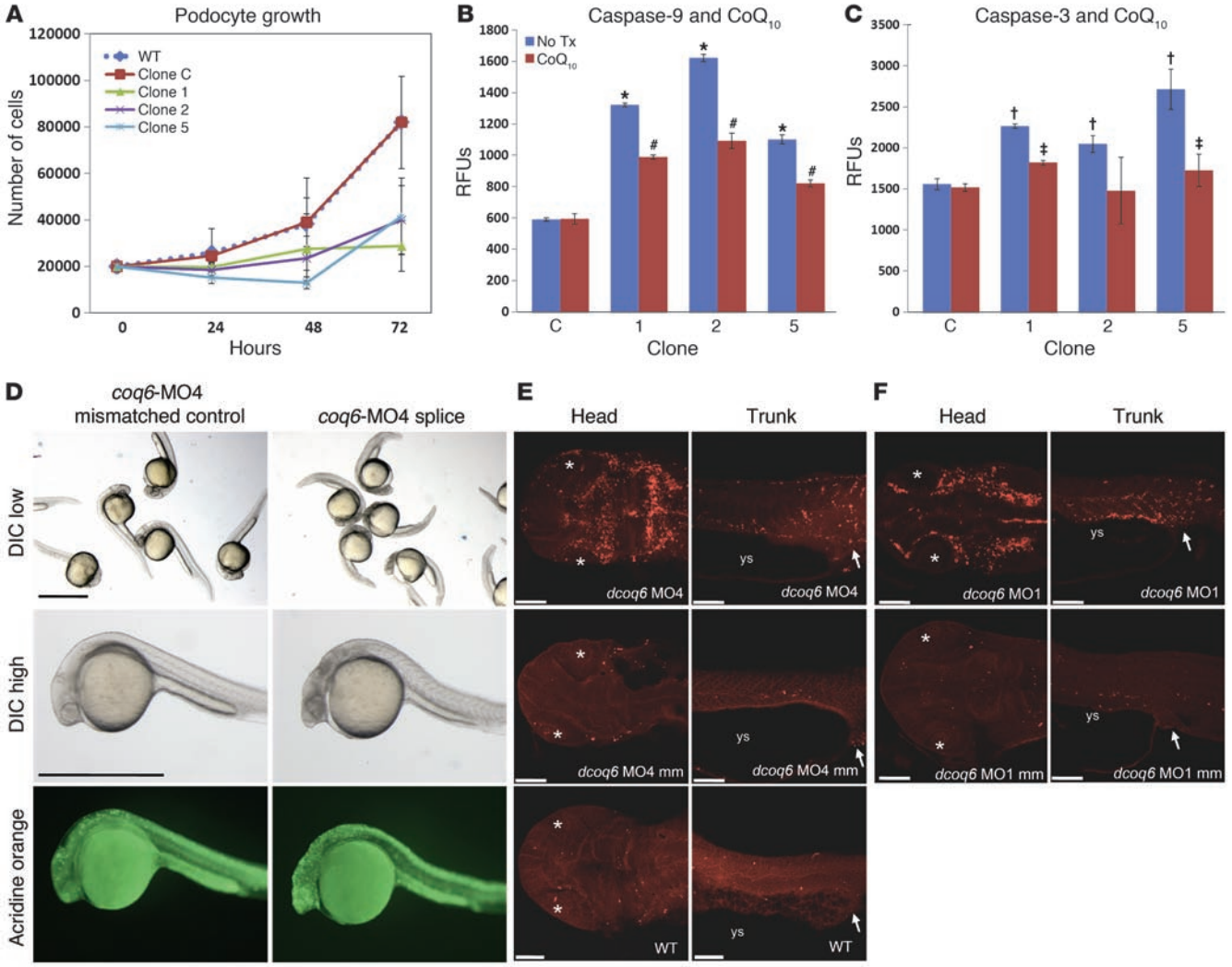

Figure 5

COQ6 knockdown causes apoptosis in podocytes and zebrafish embryos. (**A**–**C**) *Coq6* downregulation in cultured mouse podocytes induced apoptosis that was diminished by CoQ_{10} treatment. Data are mean ± SEM. (**A**) Growth curve analysis of *Coq6* knockdown clones. 20,000 podocytes were seeded per 24-well plate, plated, detached, and counted ($n = 4$). (**B** and **C**) Caspase-9 (**B**) and caspase-3 (**C**) activity in undifferentiated *Coq6* knockdown clones by FIENA before and after CoQ_{10} treatment. RFUs derived from cleaved capase-9 or caspase-3 substrate peptide were measured in lysates from 1×10^6 cells ($n = 3$). C, control clone; No Tx, no treatment. $^*P < 0.001$, $^\dagger P < 0.05$ versus control; $^\#P < 0.005$, $^\ddagger P < 0.05$ versus untreated. (**D**–**F**) *coq6* knockdown in zebrafish embryos 28 hours after fertilization increases apoptosis. (**D**) *coq6*-MO4 directed against zebrafish *coq6* intron 7 splice donor blocked proper splicing of *coq6* mRNA (see Supplemental Figure 1N). Negative controls were injected with 0.1 mM *coq6* mismatch MO. Note the gray appearance of zebrafish heads upon differential interference contrast (DIC) microscopy as a sign of increased cell death. (**E** and **F**) Zebrafish dorsal head and lateral trunk views. Embryos were injected as indicated with 0.1 mM *coq6*-MO4 splice targeting MO (**E**), MO targeting the AUG translation start site (*dcoq6* MO1; **F**), *coq6* mismatch (mm) MO negative controls, or left uninjected (WT). Cells were stained by an antibody against cleaved caspase-3, a specific marker for apoptotic cells. Lens (asterisk), yolk sac (ys), and cloaca (arrow) are indicated. Scale bars: 1 mm (**D**); 100 μm (**E** and **F**).

of *Coq6* expression in podocytes in vitro. When culturing podocyte clones 1, 2, and 5 in the presence of CoQ_{10} at a concentration of 50 μM for 48 hours, we observed a decrease in caspase-9 and caspase-3 activities (Figure 5, B and C). Compared with clones cultured in the absence of CoQ_{10}, this decrease was statistically significant ($P < 0.05$), whereas we did not detect any changes in caspase activities of negative control clones (Figure 5, B and C).

To examine *COQ6* loss of function in a vertebrate organism rather than cell lines, we performed morpholino oligonucleotide (MO) knockdown of *coq6* in zebrafish. We demonstrate that *coq6*-MO4 MOs directed against the zebrafish *coq6* intron 7 splice donor site (Supplemental Figure 1N) and the AUG translation start site induced apoptosis preferentially in heads and trunks of zebrafish embryos 28 hours after fertilization (Figure 5, D–F).

Because *COQ6* mutations cause SND, it is interesting to note that treatment with water-soluble CoQ_{10} decreased apoptosis and activated caspase-3 and improved hearing in a guinea pig model of noise-induced hearing loss (33). The kidney phenotype

of *COQ6* mutations is remarkably similar to that of mutations in *COQ2* (23) and *PDSS2* in humans (34) and *Pdss2* in mice (24), all of which respond to CoQ_{10} treatment (12, 35). Patients with defects in genes required for CoQ_{10} biosynthesis — *PDSS2*, *COQ2*, and *COQ9* — exhibit renal disease, and in some cases there is a dramatic response to CoQ_{10} therapy, but this is quite variable (36).

Discussion

In this study, we report what we believe to be a novel cause of SRNS that appears to respond to oral CoQ_{10} supplementation. CoQ_{10}, an essential component of the mitochondrial electron transport chain and one of the most potent lipophilic antioxidants (37), is also required for pyrimidine nucleoside biosynthesis and has been implicated in the inhibition of apoptosis by its prevention of inner mitochondrial membrane collapse (38). In multiple studies, the deleterious effect of CoQ_{10} deficiency to mitochondria has been shown. CoQ_{10} deficiency can lead to the opening of the mitochondrial permeability transition pore (MPTP) directly, but an increased amount of ROS caused by CoQ_{10} deficiency can also induce the MPTP by opening of nonspecific high-conductance permeability transition pores in the mitochondrial inner membrane (39). Experiments in HEK293 cells recently showed that CoQ_{10} inhibits Bax-induced mitochondrial dysfunction and protects mitochondria from permeability transition pore opening (9). Here, we confirmed that *COQ6* mutations that cause CoQ_{10} deficiency led to the upregulation of proapoptotic factors. Interestingly, CsA inhibits the MPTP through interaction with cyclophilin D, an essential component of the MPTP (40). We showed that incubation of *COQ6* knockdown podocytes with CsA had a mild rescue effect and decreased activity of caspase-3. Patient A1072-22, who had been treated with CsA in the past, also showed partial remission of proteinuria after treatment with CsA.

Mutations in 5 other CoQ_{10} biosynthesis enzymes leading to CoQ_{10} deficiency have been recently implicated in other monogenic mitochondriopathies, generally characterized by central nervous system signs and myopathy (22, 34, 41–43); 1 patient with mutations in *PDSS2* and 5 patients with mutations in *COQ2* also presented with SRNS (22, 34, 43). So far, the exact pathogenic mechanism has remained unclear. Interestingly, 1 patient with mutations in *COQ2* was successfully treated with oral CoQ_{10} supplementation, showing progressive recovery of renal function and a reduced level of proteinuria until 5 years after completion of treatment (22). The podocyte-specific phenotype caused by *PDSS2* mutations leading to primary CoQ_{10} deficiency was demonstrated in the *Pdss2* knockout mouse (24). Conditional knockouts targeted to renal tubular epithelium, monocytes, or hepatocytes did not show disease manifestation. It remains unclear why the podocyte in particular is affected by *PDSS2*-dependent CoQ_{10} deficiency.

Interestingly, the presentation of primary CoQ_{10} deficiency caused by genetic mutations is very heterogeneous. It seems that the mutations in *PDSS2* and *COQ2* are partial loss-of-function mutations. Therefore, the phenotypes (ATP synthesis, ROS production) may depend on the content of Q in the cell, which is determined by the severity of the mutation. Mutations in *PDSS2*, for example, cause reduced ATP synthesis in cultured fibroblasts, but no increase in ROS production, whereas mutations in *COQ2* cause no difference in ATP synthesis in cultured fibroblasts, but increase ROS production (36). One could speculate that different cell types and/or tissues react differently to ROS and ATP synthesis defects according to their antioxidant defense mechanisms or the level of respiratory activity, explaining the wide spectrum of clinical features. Based on the surprising Golgi localization of COQ6, COQ7, and COQ9, we speculate that the antioxidant function of Q/QH2 in certain cells, such as podocytes, may depend on targeted synthesis of CoQ in the Golgi for delivery to the plasma membrane, which in the podocyte constitutes an enormous surface area that must contain vulnerable lipid components. Whereas most other forms of monogenic childhood NS are characterized by a lack of response to therapy (10, 16, 17, 44), the identification by mutation analysis of individuals with NS caused by CoQ_{10} biosynthesis defects, as described here, is important because those individuals may respond to treatment with CoQ_{10}.

Methods

Subjects

We obtained blood, tissue samples, and pedigrees following informed consent from individuals with NS and/or from their parents. Human subject research was approved by the University of Michigan Institutional Review Board. The diagnosis of NS was made by a pediatric nephrologist based on either chronic or recurrent high-grade proteinuria (>40 mg/m^2/h) or persistent low-grade proteinuria (>4 mg/m^2/h) (45). Steroid-sensitive NS and SRNS were defined according to standard criteria (45, 46). Renal biopsies were evaluated by a reference renal pathologist. Age at onset of ESRF was defined as age at first renal replacement therapy, i.e., dialysis or renal transplantation. Clinical data were obtained using a standardized questionnaire (www.renalgenes.org).

Genetic mapping and exon sequencing

We performed a genome-wide search for linkage by homozygosity mapping using the 250k Affymetrix SNP microarray (47). Data were evaluated by calculating nonparametric lod scores and scoring for homozygosity (Z_{hom}) across the whole genome in order to identify regions of homozygosity. The GENEHUNTER-MODSCORE program (48) was used to calculate multipoint lod scores assuming recessive inheritance with complete penetrance, a disease allele frequency of 0.001, and the marker allele frequencies for individuals of mixed European descent specified by Affymetrix. Parametric and nonparametric lod scores were plotted over genetic distance across the entire human genome using GNUPLOT software (http://www.gnuplot.info/). See Supplemental Table 2 for exon sequencing primers.

COQ6 mRNA expression

The probe for human Northern blot analysis was obtained by digesting the *COQ6* isoform a coding region cloned into pCRIITOPO with *EcoRI* and was radiolabeled with α-^{32}P dCTP (Amersham Biosciences) using the Random Primers DNA Labeling System kit (Invitrogen) and successively purified with Quick-Spin columns (Roche) according to the manufacturer's protocol. Radiolabeled probes were hybridized to a commercial preblotted membrane (FirstChoice Human Blot 1 membrane; Ambion) containing 2 μg/lane poly(A)$^+$ RNA from 10 human tissues. Prehybridization and hybridization were both performed in a 50% formamide buffer at 42°C, with a working concentration of 1.5×10^6 cpm and 0.1 mg salmon sperm DNA per milliliter. The excess probe was removed by washing at 65°C for 15 minutes using a 0.1% SDS, 0.1× sodium chloride–sodium citrate buffer solution. Radioactivity was detected with a Storm PhosphoImager (Molecular Dynamics) after overnight exposure. Selective amplification of *COQ6* isoform b was carried out using primers in exon 1b and in exon 4. Simultaneous amplification of isoform a and isoform b was carried out using primers on exon 2 and on exon 4. PCR conditions were 94°C for 3 minutes followed by 35 cycles of 94°C for 30 seconds,

55°C for 30 seconds, and 72°C for 30 seconds and a final extension step of 72°C for 7 minutes. Amplified fragments were also purified from agarose gel and sequenced. Primer sequences were as follows: exon 1b forward, 5′-TCTAGCTTTGGCGTCTGGTT-3′; exon 2 forward, 5′-CTTCTAAGCTTGATATGATATTCACTTTCATGACAAG-3′; exon 4 reverse, 5′-CTTCTGGATCCATGATGACATCATTCTCCAC-3′.

Generation of plasmids

Yeast *COQ6* was amplified from genomic DNA extracted from a WT BY4741 strain and cloned in pCM189 vector. Site-specific mutagenesis was performed using the QuickChange kit (Stratagene) according to the manufacturer's protocol. To generate constructs that expressed the gene under the control of the endogenous yeast *coq6* promoter, the different pCM189–yeast COQ6 constructs were digested with *SacI* and *MscI* (to eliminate the CYC1 promoter and control elements); religated with a fragment encompassing the yeast COQ6 promoter, the 5′ end of the gene, and the *MscI* site; amplified from genomic DNA; and cut accordingly. Plasmid maps were described previously (49). Yeast growth and transformation were performed as described below.

COQ6-GFP expression studies

The complete coding region of full-length human *COQ6* isoform a, lacking termination codon but including the Kozak sequence, was PCR amplified from pCRIITOPO-COQ6 and subcloned into the *HindIII* and *BamHI* sites of pEGFP-N1 (BD Biosciences — Clontech). The correctness of the construct was verified by direct sequencing. HeLa cells stably expressing mitochondrially targeted red fluorescent protein (50) were grown on coverslips in complete DMEM (Sigma-Aldrich) containing 10% fetal bovine serum until 70% confluent, then transfected with the purified plasmid using Effectene Transfection Reagent (Qiagen) according to the manufacturer's instructions. Cells were visualized after 48 hours using a Nikon Video Confocal microscope.

In situ hybridization analysis in mice

Whole-mount in situ hybridization was performed following a standard procedure with digoxigenin-labeled antisense riboprobes (51). Stained specimens were transferred in 80% glycerol prior to documentation. In situ hybridization on 10-μm paraffin sections was done as described previously (52).

Immunofluorescence

Rat kidneys were perfusion-fixed with paraformaldehyde/lysine/periodate and processed as previously described (3). For absorption experiments, the immunopurified α–COQ6-TPEP2, COQ7, and COQ9 antibodies were preabsorbed with an equal weight of cognate or noncognate peptide overnight at 4°C. The following antibodies were used: WT1 mouse monoclonal antibody (catalog no. sc-7385; Santa Cruz Biotechnology Inc.); PLCe1 goat polyclonal antibody (catalog no. sc-28404; Santa Cruz Biotechnology Inc.); α–COQ6-TPEP2 immunopurified rabbit antipeptide antibody (against peptide sequence N-DKDNLDDMGYIVEND-C; anti-rat Glepp1 mouse monoclonal antibody (1B4; ref. 53), CoQ7 goat polyclonal antibody (catalog no. sc-66353; Santa Cruz Biotechnology Inc.); CoQ9 rabbit polyclonal antibody (catalog no. 14874-1-AP; Protein Tech); TGN38 monoclonal mouse antibody (catalog no. 610898; BD Biosciences); and GM130 mouse monoclonal antibody (catalog no. 610823; BD Biosciences).

Yeast studies

Yeast growth. The *S. cerevisiae coq6*-null mutants W303ΔG63 (Mat α ade2-1 his 3-1,15 leu2-3,112 trp1-1 ura3-1 ΔCOQ6:HIS3; ref. 18) and W303ΔCOQ8 (Mat α ade2-1 his 3-1,15 leu2-3,112 trp1-1 ura3-1 ΔABC1/COQ8:HIS3; ref. 54) were used in this study. Yeast growth media were prepared as described previously (55): YPD, containing 1% yeast extract, 2% peptone, and 2% dextrose; YPGal, containing 1% yeast extract, 2% peptone, 2% galactose, and 0.1% dextrose; YPG, containing 1% yeast extract, 2% peptone, and 3% glycerol; and SD-Ura, containing 0.18% nitrogen base without amino acids, 2% dextrose, 0.14% NaH_2PO_4, 0.5% $(NH_4)_2SO_4$, and a complete amino acid supplement (56), minus uracil. Solid plate media contained 2% agar.

Yeast transformation. Yeast was subjected to transformation as described previously (57), with either a low–copy number (pQM; ref. 58) or a high–copy number (pRCM; ref. 59) yeast expression plasmid. These vectors were used to prepare plasmids containing the human *COQ6* open reading frame with an in-frame aminoterminal yeast mitochondrial leader sequence (pQM_hCOQ6-MLS and pRCM_hCOQ6-MLS). Each of the following mutations in human *COQ6* were introduced by site-directed mutagenesis (Stratagene): R162X, W188X, G255R, A353D, W447X, and Q461fsX478. See Supplemental Table 1 for a complete list of plasmids used in yeast transformation experiments.

Lipid extraction and analysis. Yeast cells were grown in YPGal and harvested during log phase growth (1.0 OD_{600nm}). Lipid extracts were prepared from yeast whole cells as described previously (60). Lipids were separated by reverse-phase high-performance liquid chromatography with a Phenylhexyl column (Phenomenex 5-μm, 100 × 4.6 mm). The column was equilibrated with a mobile phase consisting of 95:5 methanol/2-propanol with 2.5 mM ammonium formate as solvent A and a flow rate of 650 μl/min. Upon sample injection, the percentage of solvent B (2-propanol with 2.5 mM ammonium formate) was increased linearly from 0% to 5% over 6 minutes, and the flow rate was also increased linearly to 800 μl/min. The flow rate and mobile phase were linearly changed back to initial conditions by 8 minutes. Q was quantified with an Applied Biosystems-MDS Sciex 4000 Q Trap (hybrid triple-quad linear ion trap analyzer with autosampler and a Turbo-V source equipped with ESI and APCI sources) as described previously (35). The samples were analyzed in multiple reaction monitoring (MRM) mode; MRM transitions were as follows: m/z 591.6/197.1 for Q_6; m/z 610.6/197.1 for Q_6H_2 with ammonium adduct; m/z 455.6/197.1 for Q_4 (Sigma-Aldrich), used as internal standard.

Podocyte expression studies

Preparation of CoQ_{10} solution for use in cell culture. Pure CoQ_{10} in powder form (Kaneka Corp.) was dissolved in 1 ml of molecular biology–grade isopropanol at a concentration of 10 mM by heating it briefly in a 95°C water bath. Thereafter, the CoQ_{10} solution was diluted 1:10 in podocyte culture media to a final stock concentration of 1 mM and reheated for an additional 5 minutes at 95°C with gentle shaking. This CoQ_{10} stock solution was stored at 4°C, protected from light for up to 4 weeks, and diluted immediately before use at 1:20 in cell culture medium to a final working concentration of 50 μM.

Podocyte culture. Immortalized murine podocytes were cultured as described previously (29). For treatment studies of undifferentiated podocytes, cells were incubated in the presence of 50 μM CoQ_{10}, 1 μM dexamethasone (Sigma-Aldrich), or 1 μM CsA (Sigma-Aldrich) for 48 hours. For analysis of differentiated podocytes, undifferentiated podocytes were cultured under nonpermissive conditions in the presence of 1 μM dexamethasone for 14 days. Cultivation was then continued in the absence of dexamethasone for an additional 48 hours. For determination of cell number and growth curve analysis, cells were seeded in 24-well plates at 20,000 cells/well. After 24, 48, or 72 hours, cells were trypsinized and counted using a hemocytometer. Experiments were done 4 times with at least 3 internal replicates.

COQ6 RNAi

For the targeted downregulation of protein expression in podocytes, we used the pSuper RNAi System (OligoEngine) (28) following the manufacturer's instructions and as done previously (61). Briefly, we cloned a 60-nt oligo including a 19-nt *COQ6* target sequence and a hairpin (5′-TTCAAGA-

GA-3′) into a modified pSuper vector, which also encoded for a zeocin selection marker (61). After transfection of undifferentiated podocytes using FuGene 6 (Roche) followed by zeocin selection at 500 μg/ml for 7–10 days, appearing podocyte clones were covered by cloning chambers, trypsinized, and expanded separately from each other in culture medium containing 100 μg/ml zeocin. In total, 5 different *COQ6* targeting sequences were used (clone 1, AACAGAGTCAGCTCCATAT; clone 2, AATGACGTCATCATGTATG; clone 3, CTGTGGCAGATCGAGTGAA; clone 4, AACTGTTGATTGGTGCTGA; clone 5, AAGGACTTAGGCTCCATGA) as well as 1 scrambled control sequence (5′-CCGCGACTCGCCGTCTGCG-3′). Stable transfected clones were expanded and used for RNA isolation and functional studies.

RNA isolation and RT-PCR

RNA was isolated from 2×10^6 undifferentiated podocytes using the RNeasy kit (Qiagen) following the manufacturer's protocol. Prior to RT-PCR, total RNA samples were digested with DNase I (Roche) and RNA was transcribed into cDNA using Superscript II (Invitrogen). For RT-PCR, 100 ng cDNA, AmpliTaq Gold DNA polymerase (Applied Biosystems), and sequence-specific, intron-spanning primers were used (COQ6 forward, CAGACACCGTGTACGACGTG; COQ6 reverse, CCAACAGCTTTGCTCTCATAGAG; GAPDH forward, TATGTCGTGGAGTCTACTGG; GAPDH reverse, AGTGATGGCATGGACTGTGG). 30 PCR cycles (5 minutes at 95°C, 30 seconds at 53°C, and 30 seconds at 72°C) were run on a GeneAmp PCR System 9700 (Applied Biosystems). PCR reactions were analyzed on a 2% agarose gel, and ethidium bromide signals were captured with a Bio-Rad Gel Doc XR system.

Inner $\Delta\Psi m$

To analyze changes in the $\Delta\Psi$m of undifferentiated podocytes, we used TMRE (Invitrogen) as described previously (62). Briefly, 3×10^5 cells were trypsinized and incubated in 25 nM TMRE for 30 minutes at 37°C. With this concentration (nonquenching mode), depolarization causes a drop in TMRE fluorescence. Cells were washed with PBS and analyzed by flow cytometry (FACSCalibur; BD), measuring TMRE fluorescence in FL-2. The relative fluorescence of TMRE was compared with that of the respective untreated control cells in each experiment. 3 replicates were analyzed per treatment group.

FIENA

To determine caspase-3 and -9 activities in podocyte extracts, we used the Fluorometric Assay Kits from BioVision according to the manufacturer's protocol. In brief, podocytes were cultured in 6- or 12-well plates, trypsinized, and counted using a hemocytometer. 1×10^5 to 1×10^6 cells were lysed on ice for 10 minutes, and the derivatized peptide DEVD–7-amino-4-trifluoromethyl coumarin (DEVD-AFC) caspase-3 or -9 cleavage substrate was added at a final concentration of 50 μM in 2× reaction buffer containing 10 mM dithiothreitol. The reaction was incubated at 37°C for 1–24 hours, and green fluorescence (λ_{max}, 505 nm) of free AFC after caspase-3– or caspase-9–mediated cleavage was measured in relative fluorescence units (RFU) using a fluorometer (SpectraMax M5; Molecular Devices) at different time points. Values were normalized to cell lysates without substrate and to substrate in reaction buffer in the absence of cell lysate. Experiments were done 3 times with at least 3 internal replicates.

Zebrafish MO-mediated knockdown

MOs were obtained from Gene Tools. The nucleotide sequences of the translation-blocking (coq6-MO1) and splice-blocking (coq6-MO4) MOs against *D. rerio coq6* were 5′-GCTTAGCTTTAGCCAGAGACAGCAT-3′ and 5′-ACACATAAGGTCAGCTCACGGGAAG-3′, respectively. The 5-bp mismatch controls for the MOs were as follows: coq6-MO1mm, 5′-GGTTACCTTTACCCAGACACACCAT-3′; coq6-MO4mm, 5′-ACAGATAACGTCACCTCAGGGCAAG-3′. Fertilized eggs were microinjected with the specified amount of MO dissolved in 0.1M KCl. For immunohistochemical labeling, embryos were fixed with 4% PFA in PBS (pH 7.4) and stained with antibody against activated caspase-3 (1:200; BD Biosciences) following standard protocols (63).

Statistics

To evaluate caspase-3 and -9 activity in cell lines, Pearson χ^2 test was used with a critical *P* value of 0.05 (Figure 5).

Databases

Genetic mapping was performed using http://genome.ucsc.edu (May 2004 freeze).

Accession numbers

Accession numbers of *COQ6* orthologs were NP_872282 for *Homo sapiens*, NP_001038869 for *D. rerio*, and ZP_00723222 *E. coli*.

Acknowledgments

We thank the affected individuals and their families for participation. We thank Corina Nailescu for contribution of clinical data. This research was supported by grants from the NIH to F. Hildebrandt (DK076683 and DK086542), C.F. Clarke (GM45952), and R.C. Wiggins (DK46073 and P30 DK081943) and by a grant from the KMD Foundation and the Thrasher Research Fund to F. Hildebrandt. F. Hildebrandt is an Investigator of the Howard Hughes Medical Institute, a Doris Duke Distinguished Clinical Scientist, and the Frederick G.L. Huetwell Professor. H. Prokisch was supported by the Impulse and Networking Fund of the Helmholtz Association in the framework of the Helmholtz Alliance for Mental Health in an Ageing Society (HA-215), by the German Network for Mitochondrial Disorders (mitoNET 01GM0862 and 01GM0867), and by Systems Biology of Metabotypes (SysMBo 0315494A). The work was further supported by a grant from the German Research Foundation (DFG, SFB 423, TP B19) to M. Zenker, by the German Federal Ministry of Science and Education through the National Genome Research Network to G. Nürnberg and P. Nürnberg, by the European Community FP7 program (EUNEFRON 201590) to D. Müller, by Fondazione CARIPARO Telethon Italy (GGP09207) to L. Salviati, by a Spanish FIS grant (PI080500) to P. Navas, and by the Young Investigator Career Development Grant from the NephCure Foundation and the National Scientist Development Grant from the American Heart Association to C. Faul.

Received for publication November 6, 2010, and accepted in revised form February 9, 2011.

Address correspondence to: Friedhelm Hildebrandt, Howard Hughes Medical Institute, Departments of Pediatrics and Human Genetics, University of Michigan Health System, 8220C MSRB III, 1150 West Medical Center Drive, Ann Arbor, Michigan 48109-5646, USA. Phone: 734.615.7285; Fax: 734.615.1386; E-mail: fhilde@umich.edu.

1. Kestila M, et al. Positionally cloned gene for a novel glomerular protein--nephrin--is mutated in congenital nephrotic syndrome. *Mol Cell.* 1998;1(4):575–582.
2. Boute N, et al. NPHS2, encoding the glomerular protein podocin, is mutated in autosomal recessive steroid-resistant nephrotic syndrome. *Nat Genet.* 2000;24(4):349–354.
3. Hinkes B, et al. Positional cloning uncovers mutations in PLCE1 responsible for a nephrotic syndrome variant that may be reversible. *Nat Genet.* 2006; 38(12):1397–1405.
4. Kaplan JM, et al. Mutations in ACTN4, encoding

alpha-actinin-4, cause familial focal segmental glomerulosclerosis. *Nat Genet*. 2000;24(3):251–256.
5. Reiser J, et al. TRPC6 is a glomerular slit diaphragm-associated channel required for normal renal function. *Nat Genet*. 2005;37(7):739–744.
6. Winn MP, et al. A mutation in the TRPC6 cation channel causes familial focal segmental glomerulosclerosis. *Science*. 2005;308(5729):1801–1804.
7. Brown EJ, et al. Mutations in the formin gene INF2 cause focal segmental glomerulosclerosis. *Nat Genet*. 2010;42(1):72–76.
8. Somlo S, Mundel P. Getting a foothold in nephrotic syndrome. *Nat Genet*. 2000;24(4):333–335.
9. Machuca E, Benoit G, Antignac C. Genetics of nephrotic syndrome: connecting molecular genetics to podocyte physiology. *Hum Mol Genet*. 2009; 18(R2):R185–R194.
10. Ruf RG, et al. Patients with mutations in NPHS2 (podocin) do not respond to standard steroid treatment of nephrotic syndrome. *J Am Soc Nephrol*. 2004; 15(3):722–732.
11. Weber S, et al. NPHS2 mutation analysis shows genetic heterogeneity of steroid-resistant nephrotic syndrome and low post-transplant recurrence. *Kidney Int*. 2004;66(2):571–579.
12. Montini G, Malaventura C, Salviati L. Early coenzyme Q10 supplementation in primary coenzyme Q10 deficiency. *N Engl J Med*. 2008;358(26):2849–2850.
13. Wiggins RC. The spectrum of podocytopathies: a unifying view of glomerular diseases. *Kidney Int*. 2007;71(12):1205–1214.
14. Hinkes BG, et al. Nephrotic syndrome in the first year of life: two thirds of cases are caused by mutations in 4 genes (NPHS1, NPHS2, WT1, and LAMB2). *Pediatrics*. 2007;119(4):e907–e919.
15. Karle SM, Uetz B, Ronner V, Glaeser L, Hildebrandt F, Fuchshuber A. Novel mutations in NPHS2 detected in both familial and sporadic steroid-resistant nephrotic syndrome. *J Am Soc Nephrol*. 2002;13(2):388–393.
16. Hasselbacher K, et al. Recessive missense mutations in LAMB2 expand the clinical spectrum of LAMB2-associated disorders. *Kidney Int*. 2006;70(6):1008–1012.
17. Mucha B, et al. Mutations in the Wilms' tumor 1 gene cause isolated steroid resistant nephrotic syndrome and occur in exons 8 and 9. *Pediatr Res*. 2006; 59(2):325–331.
18. Gin P, et al. The Saccharomyces cerevisiae COQ6 gene encodes a mitochondrial flavin-dependent monooxygenase required for coenzyme Q biosynthesis. *J Biol Chem*. 2003;278(28):25308–25316.
19. DiMauro S, Mancuso M. Mitochondrial diseases: therapeutic approaches. *Biosci Rep*. 2007;27(1–3):125–137.
20. Hyun DH, Hernandez JO, Mattson MP, de Cabo R. The plasma membrane redox system in aging. *Ageing Res Rev*. 2006;5(2):209–220.
21. DiMauro S, Quinzii CM, Hirano M. Mutations in coenzyme Q10 biosynthetic genes. *J Clin Invest*. 2007; 117(3):587–589.
22. Diomedi-Camassei F, et al. COQ2 nephropathy: a newly described inherited mitochondriopathy with primary renal involvement. *J Am Soc Nephrol*. 2007; 18(10):2773–2780.
23. Lopez-Martin JM, et al. Missense mutation of the COQ2 gene causes defects of bioenergetics and de novo pyrimidine synthesis. *Hum Mol Genet*. 2007; 16(9):1091–1097.
24. Peng M, et al. Primary coenzyme Q deficiency in Pdss2 mutant mice causes isolated renal disease. *PLoS Genet*. 2008;4(4):e1000061.
25. Salviati L, et al. Infantile encephalomyopathy and nephropathy with CoQ10 deficiency: a CoQ10-responsive condition. *Neurology*. 2005;65(4):606–608.
26. Tryggvason K, Patrakka J, Wartiovaara J. Hereditary proteinuria syndromes and mechanisms of proteinuria. *N Engl J Med*. 2006;354(13):1387–1401.
27. Padilla-Lopez S, Jimenez-Hidalgo M, Martin-Montalvo A, Clarke CF, Navas P, Santos-Ocana C. Genetic evidence for the requirement of the endocytic pathway in the uptake of coenzyme Q6 in Saccharomyces cerevisiae. *Biochim Biophys Acta*. 2009; 1788(6):1238–1248.
28. Brummelkamp TR, Bernards R, Agami R. A system for stable expression of short interfering RNAs in mammalian cells. *Science*. 2002;296(5567):550–553.
29. Mundel P, et al. Rearrangements of the cytoskeleton and cell contacts induce process formation during differentiation of conditionally immortalized mouse podocyte cell lines. *Exp Cell Res*. 1997; 236(1):248–258.
30. Green DR. Apoptotic pathways: ten minutes to dead. *Cell*. 2005;121(5):671–674.
31. Wilson MR. Apoptosis: unmasking the executioner. *Cell Death Differ*. 1998;5(8):646–652.
32. Green DR, Kroemer G. The pathophysiology of mitochondrial cell death. *Science*. 2004; 305(5684):626–629.
33. Fetoni AR, Piacentini R, Fiorita A, Paludetti G, Troiani D. Water-soluble Coenzyme Q10 formulation (Q-ter) promotes outer hair cell survival in a guinea pig model of noise induced hearing loss (NIHL). *Brain Res*. 2009;1257:108–116.
34. Lopez LC, et al. Leigh syndrome with nephropathy and CoQ10 deficiency due to decaprenyl diphosphate synthase subunit 2 (PDSS2) mutations. *Am J Hum Genet*. 2006;79(6):1125–1129.
35. Saiki R, et al. Coenzyme Q10 supplementation rescues renal disease in Pdss2kd/kd mice with mutations in prenyl diphosphate synthase subunit 2. *Am J Physiol Renal Physiol*. 2008;295(5):F1535–F1544.
36. Quinzii CM, et al. Respiratory chain dysfunction and oxidative stress correlate with severity of primary CoQ10 deficiency. *FASEB J*. 2008;22(6):1874–1885.
37. Bentinger M, Brismar K, Dallner G. The antioxidant role of coenzyme Q. *Mitochondrion*. 2007; 7(suppl):S41–S50.
38. Turunen M, Olsson J, Dallner G. Metabolism and function of coenzyme Q. *Biochim Biophys Acta*. 2004; 1660(1–2):171–199.
39. Kim I, Rodriguez-Enriquez S, Lemasters JJ. Selective degradation of mitochondria by mitophagy. *Arch Biochem Biophys*. 2007;462(2):245–253.
40. Waldmeier PC, Zimmermann K, Qian T, Tintelnot-Blomley M, Lemasters JJ. Cyclophilin D as a drug target. *Curr Med Chem*. 2003;10(16):1485–1506.
41. Lagier-Tourenne C, et al. ADCK3, an ancestral kinase, is mutated in a form of recessive ataxia associated with coenzyme Q10 deficiency. *Am J Hum Genet*. 2008; 82(3):661–672.
42. Duncan AJ, et al. A nonsense mutation in COQ9 causes autosomal-recessive neonatal-onset primary coenzyme Q10 deficiency: a potentially treatable form of mitochondrial disease. *Am J Hum Genet*. 2009; 84(5):558–566.
43. Mollet J, et al. Prenyldiphosphate synthase, subunit 1 (PDSS1) and OH-benzoate polyprenyltransferase (COQ2) mutations in ubiquinone deficiency and oxidative phosphorylation disorders. *J Clin Invest*. 2007;117(3):765–772.
44. Antignac C. Molecular basis of steroid-resistant nephrotic syndrome. *Nefrologia*. 2005; 25(suppl 2):25–28.
45. [No authors listed]. Short versus standard prednisone therapy for initial treatment of idiopathic nephrotic syndrome in children. *Lancet*. 1988;1(8582):380–383.
46. ISKDC. Primary nephrotic syndrome in children: Clinical significance of histopathologic variants of minimal change and of diffuse mesangial hypercellularity: A Report of the International Study of Kidney Disease in Children. *Kidney Int*. 1981;20(6):765–771.
47. Hildebrandt F, et al. A systematic approach to mapping recessive disease genes in individuals from outbred populations. *PloS Genet*. 2009;5(1):e1000353.
48. Strauch K. Parametric linkage analysis with automatic optimization of the disease model parameters. *Am J Hum Genet*. 2003;73(suppl 1):A2624.
49. Gari E, Piedrafita L, Aldea M, Herrero E. A set of vectors with a tetracycline-regulatable promoter system for modulated gene expression in *Saccharomyces cerevisiae*. *Yeast*. 1997;13(9):837–848.
50. Casarin A, et al. Functional characterization of human COQ4, a gene required for Coenzyme Q10 biosynthesis. *Biochem Biophys Res Commun*. 2008;372(1):35–39.
51. Wilkinson DG. Whole mount in situ hybridization of vertebrate embryos. In: Wilkinson DG, ed. *In Situ Hybridization: A Practical Approach*. Oxford, United Kingdom: IRL Press; 1992:75–83.
52. Franco D, de Boer PA, de Gier-de Vries C, Lamers WH, Moorman AF. Methods on in situ hybridization, immunohistochemistry and beta-galactosidase reporter gene detection. *Eur J Morphol*. 2001; 39(3):169–191.
53. Yang DH, et al. Glomerular epithelial protein 1 and podocalyxin-like protein 1 in inflammatory glomerular disease (crescentic nephritis) in rabbit and man. *Lab Invest*. 1996;74(3):571–584.
54. Do TQ, Hsu AY, Jonassen T, Lee PT, Clarke CF. A defect in coenzyme Q biosynthesis is responsible for the respiratory deficiency in *Saccharomyces cerevisiae abc1* mutants. *J Biol Chem*. 2001;276(21):18161–18168.
55. Burke D, Dawson D, Stearns T. *Methods in Yeast Genetics*. Plainview, New York, USA: Cold Spring Harbor Laboratory Press; 2000.
56. Poon WW, et al. Yeast and rat Coq3 and *Escherichia coli* UbiG polypeptides catalyze both O-methyltransferase steps in coenzyme Q biosynthesis. *J Biol Chem*. 1999;274(31):21665–21672.
57. Elble R. A simple and efficient procedure for transformation of yeasts. *Biotechniques*. 1992;13(1):18–20.
58. Hsu AY, Poon WW, Shepherd JA, Myles DC, Clarke CF. Complementation of *coq3* mutant yeast by mitochondrial targeting of the *Escherichia coli* UbiG polypeptide: evidence that UbiG catalyzes both *O*-methylation steps in ubiquinone biosynthesis. *Biochemistry*. 1996;35(30):9797–9806.
59. Xie LX, et al. Expression of the human atypical kinase *ADCK3* rescues coenzyme Q biosynthesis and phosphorylation of Coq polypeptide in yeast *coq8* mutants [published online ahead of print February 3, 2011]. *Biochim Biophys*. doi:10.1016/j.bbalip.2011.01.009.
60. Jonassen T, Clarke CF. Isolation and functional expression of human *COQ3*, a gene encoding a methyltransferase required for ubiquinone biosynthesis. *J Biol Chem*. 2000;275(17):12381–12387.
61. Asanuma K, et al. Synaptopodin regulates the actin-bundling activity of alpha-actinin in an isoform-specific manner. *J Clin Invest*. 2005;115(5):1188–1198.
62. Krick S, et al. Mpv17l protects against mitochondrial oxidative stress and apoptosis by activation of Omi/HtrA2 protease. *Proc Natl Acad Sci U S A*. 2008; 105(37):14106–14111.
63. Zhou W, Dai J, Attanasio M, Hildebrandt F. Nephrocystin-3 is required for ciliary function in zebrafish embryos. *Am J Physiol Renal Physiol*. 2010; 299(1):F55–F62.